Brain Tumor Cells in Circulation Are Enriched for Mesenchymal Gene Expression

Published in final edited form as:
Cancer Discov. 2014 November ; 4(11): 1299–1309. doi:10.1158/2159-8290.CD-14-0471.

Brain Tumor Cells in Circulation are Enriched for Mesenchymal Gene Expression

James P. Sullivan[1,3,*], **Brian V. Nahed**[1,4,*], **Marissa W. Madden**[1], **Samantha M. Oliveira**[1], **Simeon Springer**[1], **Deepak Bhere**[5], **Andrew S. Chi**[1,5], **Hiroaki Wakimoto**[1,4], **S. Michael Rothenberg**[1,3], **Lecia V. Sequist**[1,3], **Ravi Kapur**[2], **Khalid Shah**[5,6], **A. John Iafrate**[1,7], **William T. Curry**[1,4], **Jay S. Loeffler**[1], **Tracy T. Batchelor**[1,5], **David N. Louis**[1,7], **Mehmet Toner**[2,8], **Shyamala Maheswaran**[1,8,†], and **Daniel A. Haber**[1,3,9,†]

[1]Massachusetts General Hospital Cancer Center, Harvard Medical School, Boston, Massachusetts 02114, USA

[2]Center for Engineering in Medicine, Harvard Medical School, Boston, Massachusetts 02114, USA

[3]Department of Medicine, Harvard Medical School, Boston, Massachusetts 02114, USA

[4]Department of Neurosurgery, Harvard Medical School, Boston, Massachusetts 02114, USA

[5]Department of Neurology, Harvard Medical School, Boston, Massachusetts 02114, USA

[6]Department of Radiology, Harvard Medical School, Boston, Massachusetts 02114, USA

[7]Department of Pathology, Harvard Medical School, Boston, Massachusetts 02114, USA

[8]Department of Surgery, Harvard Medical School, Boston, Massachusetts 02114, USA

[9]Howard Hughes Medical Institute, Chevy Chase, Maryland 20815, USA

Abstract

Glioblastoma (GBM) is a highly aggressive brain cancer characterized by local invasion and angiogenic recruitment, yet metastatic dissemination is extremely rare. Here, we adapted a microfluidic device to deplete hematopoietic cells from blood specimens of patients with GBM, uncovering evidence of circulating brain tumor cells (CTCs). Staining and scoring criteria for GBM CTCs were first established using orthotopic patient-derived xenografts (PDX), and then applied clinically: CTCs were identified in at least one blood specimen from 13/33 patients (39%; 26/87 samples). Single GBM CTCs isolated from both patients and mouse PDX models demonstrated enrichment for mesenchymal over neural differentiation markers, compared with primary GBMs. Within primary GBMs, RNA-in-situ hybridization identifies a subpopulation of highly migratory mesenchymal tumor cells, and in a rare patient with disseminated GBM,

[†]Corresponding Authors: Shyamala Maheswaran, Massachusetts General Hospital Cancer Center, Building 149 13th Street, Charlestown, MA 02129. Phone: 617-726-6552; Fax: 617-726-6919; maheswaran@helix.mgh.harvard.edu. [†]Daniel A. Haber, Massachusetts General Hospital Cancer Center, Building 149 13th Street, Charlestown, MA, 02129. Phone: 617-726-7805; Fax: 617-726-6919; haber@helix.mgh.harvard.edu.
[*]Denotes equal contribution

Disclosure of Conflicts of Interest: The authors declare no potential conflicts of interests.

systemic lesions were exclusively mesenchymal. Thus, a mesenchymal subset of GBM cells invades into the vasculature, and may proliferate outside the brain.

Keywords

Glioblastoma; circulating tumor cells; metastasis; EMT

Introduction

Glioblastoma is the most common and aggressive primary malignant brain tumor, whose histological characteristics include necrosis, infiltration into surrounding brain tissue, and microvascular proliferation. Despite advances in surgical techniques, radiation and chemotherapy, recurrence is inevitable and two-year survival remains at 25%(1). Major challenges to the treatment of GBM include the inability to excise tumor cells infiltrating into normal brain tissue, the poor penetration of therapeutic agents into the central nervous system (CNS), the common difficulty in distinguishing tumor responses from recurrence using standard imaging criteria, and the inherent risks associated with brain biopsies needed to monitor tumor evolution during disease progression (2).

Despite its locally aggressive features, GBMs rarely form clinically evident extracranial metastases, with only 0.4% of cases having metastases to visceral organs, including liver, spleen, kidney, and skin (3). Under-diagnosis of subclinical lesions may contribute to the infrequent documentation of systemic metastases in GBM, but the discordance between the high degree of local invasiveness and the very rare distant spread is likely to reflect inherent biological features of the cancer. As exemplified by the “seed” versus “soil” debate (4), it is unclear whether GBM cells are incapable of invading into the vasculature or whether invasive GBM cells circulate in the blood but are unable to proliferate in tissues outside of the brain.

While CTCs have never been isolated in patients with GBM, they have been identified in the blood of patients with most types of epithelial cancers (reviewed in (5, 6). However, their isolation presents numerous technological challenges. Even in patients with advanced cancer, CTCs typically constitute one cancer cell per billion normal blood cells (one cancer cell per million leukocytes). Most CTC detection strategies rely on antibody-mediated capture targeting cell surface expression of Epithelial Cell Adhesion Molecule (EpCAM), which is not present on GBM cells. We recently developed a microfluidic device, the CTC-iChip, which efficiently achieves depletion of leukocytes from blood specimens using magnetically tagged antibodies against the leukocyte markers CD45 and CD16, thereby enriching for CTCs in an antigen-agnostic manner (7). The CTC-iChip combines, within a single microfluidic platform, (I) size-based removal of red blood cells, platelets, and excess immunomagnetic beads; (II) single file alignment of nucleated cells (leukocytes and CTCs) within a single microfluidic streamline using inertial flow dynamics;(III) sorting magnetically tagged-leukocytes into a waste channel and isolation of untagged and un-manipulated CTCs, free in solution for application of cell surface staining and molecular analysis. To test for the presence of GBM CTCs, we applied the CTC-iChip to an orthotopic

PDX GBM mouse model, and then to patients with GBM, analyzing them for characteristic molecular markers.

Results

Detection of CTCs in Orthotopic GBM Mouse Xenografts

To optimize the capture and visualization of putative GBM CTCs, we first established an orthotopic xenograft model using tagged GBM cells directly inoculated into the mouse forebrain. We used two phenotypically different patient-derived xenografted (PDX) GBM cell lines that had been directly propagated following resection, under anchorage-independent sphere culture conditions, and then maintained by serial intracranial engraftment (8). GBM8 cells exhibit primitive neuroectodermal characteristics, express the stem cell marker CD133 and proliferate rapidly as loose neurosphere aggregates *in vitro*. Inoculation of GBM8 cells into the brain of immunosuppressed NSG mice leads to a diffusely invasive tumor that spreads along white matter tracts, such as the corpus callosum (Figure 1A and 1B and Supplemental Figure 1A and 1B)(8). In contrast, GBM24 cells lack CD133 expression, overexpress EGFR, and exhibit classic, tight neurosphere morphology *in vitro*. Upon implantation into the mouse brain, they grow slowly with a nodular phenotype, including characteristic regions of intratumoral hemorrhage and tumor necrosis (Figure 1A and 1B). We infected both GBM8 and GBM24 cells with mCherry-luciferase-expressing vectors, allowing *in vivo* imaging of tumors in the brain (luciferase expression) and definitive identification of tumor cells shed into the blood (mCherry staining) (Supplementary Figure 1A and 1B).

To generate orthotopic xenografts, 10^5 tagged GBM cells were inoculated into the frontal cortex of mice, which were then serially imaged over five weeks, as they generated a primary tumor. To search for CTCs, a terminal intracardiac bleed was used to obtain 0.5 – 1 ml of blood, which was then directly processed through the CTC-iChip (7). Following the addition of immunomagnetic bead-conjugated anti-mouse CD45 (approximately 10^7 beads per ml), a 10^4 depletion of leukocytes was achieved, and potential CTCs admixed with residual leukocytes were subjected to imaging analysis. mCherry labeling of GBM cells made it possible to identify these in the CTC-iChip product with certainty, as well as validating neural-specific stains for application to patient-derived samples.

Given the heterogeneity of GBM and the unknown expression profile of putative GBM CTCs, we sought to develop a cocktail of antibodies that would identify a broad spectrum of GBM cells. To this end, we searched the GBM biomarker literature and utilized publically available microarray data on GBM tumors (9-11), cell lines and purified WBC populations to identify GBM specific markers (Figure 1C). From this process five antibodies were selected, based on their strong immunofluorescent staining of GBM8 and GBM24 cells, and their complete absence in normal blood cells. This antibody cocktail, annotated as STEAM (SOX2, Tubulin beta-3, EGFR, A2B5, and c-MET) was combined into a single immunofluorescence staining channel (Supplemental Figure 2 and Figure1D). GBM8 and GBM24 cells spiked directly into control blood specimens and processed through the CTC-iChip were recovered with a capture efficiency of 94.5 ± 3.7% and 93.6 ± 6.5%, respectively (mCherry staining), 85.4 ± 9.8% and 91.9± 3.6%, respectively (STEAM staining) (Figure

1E), and 89.7 ± 7.1% and 90.2 ± 5.9%, respectively (mCherry/STEAM staining overlap) and with minimal STEAM staining of CD45-positive leukocytes (Figure 1F).

We then applied the mCherry and STEAM stains to CTC-iChip purified blood from mice bearing GBM8-derived (n=11) and GBM24-derived brain tumors (n =5). Sham-injected mice (n =4) were used as controls. As per CTC immunofluorescence staining protocols (12), image scoring criteria were used to establish baseline signal for mCherry staining using control tumor-free mice (median background: 3.4 cells per ml, range: 0 to 8.1, mean: 3.7 ± 3.6). Given this fluorescence imaging background, a positive CTC score was established as being above a threshold of10 mCherry positive events per ml, a cutoff that is similar to that applied in previous studies of CTCs from epithelial cancers (12, 13). mCherry positive CTCs were detected above this threshold in 5/11 (45.5%) and 2/5 (40%) mice with GBM8 and GBM24 intracranial xenografts, respectively. CTC-positive GBM8 xenograft mice had a median 17.4 CTCs per ml (range: 11.0 to 27.9, mean: 18.9 ± 6.3) and the two CTC-positive GBM24 xenograft mice had 18.9 and 12.2 cells per ml (Figure 1G and 1H). In all these cases, STEAM staining of CTCs yielded nearly identical cell numbers, compared with mCherry staining, validating the multi-antibody cocktail staining of circulating human GBM cells. No gross evidence of extracranial metastases was observed in CTC-positive mice by live BLI imaging or by epifluorescent imaging during necropsy. There was also no association between the size of the intracranial tumor and the number of CTCs detected (data not shown). Taken together, *bona fide* GBM CTCs were evident in the blood of approximately half of the mice bearing one of two phenotypically distinct intracranial xenografts of human GBM.

Identification of CTCS in the Blood of Patients with GBM

Having established criteria for identifying CTCs in mice bearing GBM xenografts, we applied this platform to peripheral blood specimens from patients with GBM, according to a Massachusetts General Hospital IRB-approved protocol. For leukocyte depletion of human blood samples, anti-CD66b was added to anti-CD45, given the increased fraction of low CD45 expressing leukocytes in human, compared with mouse blood. Venous blood specimens from 33 GBM patients and 6 healthy controls were processed through the CTC-iChip and stained simultaneously using the STEAM antibody cocktail, anti-CD14, CD16 and CD45 antibodies, and DAPI nuclear stain (Figure 2A). As with the orthotopic model, we quantified the number of fluorescent events identified in healthy controls under specific staining and imaging conditions (median background: 1.9 cells per ml, range: 0 to 6.4, mean: 2.6 ± 2.8) to set an imaging threshold for CTC detection (7 STEAM-positive cells per ml). STEAM-positive cells were identified above threshold in at least one blood specimen from 13/33 (39%) of GBM patients (26/87 blood samples (30%); average 2.6 samples per patient). The number of CTCs identified in 12 patients with progressive disease in the brain (median: 11.8 cells per ml, range: 0 to 32.7; n = 23 samples) was higher than that from 21 patients with stable disease (median: 2.1 cells per ml, range: 0 to 30.3, n = 43 samples) (P < 0.001) (Figure 2B). However, univariate analysis revealed no association between detection of CTCs in at least a blood draw and other parameters, including the number of tumor foci in the brain, extent of tumor resection or tumor genotype (Supplemental Table 1 and Supplemental Table 2). While nearly all CTCs were detected in specimens collected at

various post-surgical intervals, STEAM-positive CTCs were detected above threshold in one (11.3 STEAM-positive cells per ml) of four samples collected from pre-operative GBM patients.

To verify the neoplastic origin of candidate GBM CTCs, we tested for known EGFR genetic aberrations using fluorescence in situ hybridization (FISH). CTCs captured from six patients whose tumors were known to have EGFR gene amplification (EGFR-amplified tumor cells: 73.6± 15.6%) were simultaneously tested for STEAM staining and EGFR DNA-FISH. EGFR copy gain was observed in 39/49 (79.6%) STEAM-positive cells (Figure 2C). EGFR copy gain was not observed in patient matched WBCs, nor in CTCs matched to tumors without EGFR amplification (Supplemental Figure 3). Paired analysis of the frequency of CTCs with EGFR copy gain (median: 78.9%, range: 50% to 100%, mean: 78.3 ± 19.9%) was similar to the frequency of patient matched tumor cells with EGFR copy gain (median: 72.5%, range: 55.8% to 97%, mean: 73.6%). Further, CTCs shared the relative EGFR copy gains observed in the bulk tumor (Figure 2C). While the EGFR molecular genotype of GBM CTCs and primary GBMs was concordant, CTCs appeared to be less proliferative than the primary tumor. Indeed, comparing the proliferative index of GBM CTCs with that of the matched primary tumor showed a significantly reduced Ki67 score for the STEAM-positive CTCs ($P = 0.01$) (Figure 2D).

Single Cell Expression Analysis of GBM CTCs

To compare the gene expression patterns of GBM CTCs with that of their parental tumors, we isolated unfixed single CTCs from the CTC-iChip product by immunofluorescence-guided single cell micromanipulation. Because the fixation and permeablization process for STEAM staining is not compatible for the isolation of unfixed cells with intact RNA, CTCs were identified using fluorescently labeled antibodies against the surface markers identified in our candidate GBM marker screen; EGFR, MET and CDH11. Individual CTCs were interrogated by qRT-PCR (Fluidigm) for gene expression signatures, including 25 genes selected to represent four transcriptional subtypes of GBM: Proneural, Neural, Classical and Mesenchymal (10, 14). Each subtype is defined by a transcriptional profile that has been linked with different neural lineages and disease pathophysiology (10, 14). Expression of oligodendrocytic development genes (*ASCL1, SOX2, OLIG2, DLL3*) are transcriptional hallmarks of the Proneural subtype, whereas Classical and Neural GBMs share expression of astrocytic (*GFAP, AKT2, EGFR*) and neuronal (*SYT1, SLC12A5*) differentiation marks, respectively. Mesenchymal GBMs exhibit a transcriptional pattern related to epithelial-to-mesenchymal transition (EMT) as defined for epithelial cancers, expressing astroglial differentiation and inflammatory genes (*SERPINE1, TGFB1, RELB*). The mesenchymal GBM subtype has been associated with a poor prognosis (14-16). In addition to these markers of characteristic GBM subtypes, we measured expression of embryonic stem cell markers linked to self-renewal in GBM (*PROM1, NANOG, KLF4, POU5F1*), Notch and Hedgehog signaling components, and cell proliferation markers. *GAPDH* and *ACTB* expression serves as controls for RNA quality, and to control for leukocyte contamination, we also measured expression of three leukocyte markers in the individually selected CTCs.

In total, we analyzed 15 single GBM CTCs from 7 independent patients, and 7 single CTCs from GBM8 and GBM24 xenografts. The primary CTCs were compared with their matched, microdissected parental tumor, while the xenograft-derived CTCs were compared with single tumor cells from matched xenografts as well as neurosphere cultures. Normal leukocytes contaminating the CTC product were also analyzed as controls. Unsupervised clustering analysis easily segregated CTCs from leukocytes, with leukocyte lineage markers *PTPRC* and *CD16* expressed in isolated WBCs and absent in GBM CTCs (Supplemental Figure 4A).

Compared with their matched tumors, virtually all patient-derived GBM CTCs demonstrated elevated expression of *SERPINE1*, *TGFB1*, *TGFBR2*, and *VIM*, transcriptional hallmarks of the aggressive Mesenchymal GBM subtype (10) (Figure 3A). They also showed consistent downregulation of neural and oligodendroglial lineage markers (*ASCL1*, *GFAP*, *NCAM1*, and *SOX9*), transcripts involved in Notch and Hedgehog signaling, as well as cell proliferation markers compared with their matched primary tumor specimens (Figure 3A).

Like patient-derived CTCs, circulating GBM cells isolated from PDX mice were also characterized by overexpression of the mesenchymal genes *SERPINE1*, *TGFB1*, *TGFBR2*, and *VIM*, and by reduced expression of neural lineage and proliferative markers, compared with both primary matched tumor cells and *in vitro* neurosphere cultures (Figure 3B). Consistent with their distinct tumor of origin, GBM8 CTCs retained expression of the stem cell transcript *PROM1*, which was present in single cells from the primary tumor and in neurospheres cultures. Similarly, GBM24-derived CTCs, primary tumor cells and neurospheres shared expression of *EGFR* and *SOX2* (Supplemental Figure 4B).

Expression of Mesenchymal Genes by Subsets of Primary GBM Tumor Cells

We used RNA-in-situ hybridization (RNA-ISH) to search for subpopulations of primary GBM cells that express the high mesenchymal/low neural signature of GBM CTCs. Pooled quantifiable short nucleotide probes (ViewRNA, Affymetrix) for the four mesenchymal transcripts *SERPINE1*, *TGFB1*, *TGFBR2*, and *VIM* (Fast Red) were co-hybridized with pooled probes for the five neural/proneural differentiation transcripts *ASCL1*, *GFAP*, *OLIG2*, *PDGFRA*, and *SOX2* (Fast Blue), providing a dual-color RNA-ISH assay (17). In GBM xenografts, the human-specific RNA-ISH identified only tumor cells, without staining any normal mouse brain cells. GBM cells were classified as mesenchymal (M), neural (N) or biphenotypic (N/M). Despite the diffuse infiltrative growth pattern of GBM8, compared with the more focal phenotype of GBM24, the overall fraction of N, M and N/M tumor cells was comparable in these two xenografts. GBM8 tumors were primarily comprised of N cells (mean: 41.9 ± 6.9%) and N/M cells (52.1 ± 9.0%), with a smaller fraction of M-only cells (4.9 ± 1.9%) (n = 3 xenografts) (Figure 4A). Comparable fractions for GBM24 were noted in N (mean: 53.8 ± 4.0%), N/M (33.7 ± 11.9%), and M-only cells (18.6 ± 7.9%) (n = 3 xenografts) (Figure 4B). In addition, the two xenografts showed striking patterns in the geographic distribution of M-only GBM cells: in the highly infiltrative GBM8 tumor, M cells were admixed throughout the tumor mass, but were more predominant at the invasive edge of the deep white matter tracks (mean M cells: 42.5 ± 10.6%) compared to the bulk tumor population ($P = 0.0015$) (Figure 4A). In GBM24, M-only cells were also increased in

deep white matter (mean M cells: 66.7 ± 4.7%; P =0.016), and they also surrounded the necrotic foci (palisading cells) that are characteristic of this xenograft. M-only tumor cells were significantly increased within 100 μm of necrotic foci (mean M cells: 65.9 ± 7.3%), compared with the frequency of M-only cells in the bulk GBM24 cell population (mean M cells: 18.6 ± 7.3%; P = 0.003) (Figure 4B). Notably, palisading cells surrounding hypoxic and vaso-occulusive necrotic foci in GBM are thought to be enriched for migratory and potential tumor stem cell components (18-21).

We extended this neural/mesenchymal RNA-ISH assay to FFPE sections from patients with GBM. The proportion of tumor cells staining as M, N/M or N was comparable to that observed in GBM xenografts (mean N cells: 34.6 ± 9.9%, N/M cells: 51.5 ± 14.9%, M cells: 14.0 ± 12.1%, n = 7). Similarly, most GBM cells expressing only mesenchymal transcripts were present in perinecrotic foci enriched in palisading cells (mean M cells: 65.0 ± 5.7%), compared with the frequency of M-only cells in the total tumor cell population (mean M cells: 14.1 ± 12.1%; P = 0.014) (Figure 4C).

GBM CTCs in a patient with multiple visceral metastases

Together, the characterization of CTCs from patients and xenografts suggests that, despite the absence of visceral metastases, brain tumor cells are detectable within the bloodstream, where they express a more mesenchymal and less differentiated phenotype than the matched parental tumor. Despite the rarity of patients with metastatic GBM lesions, one such case was available for molecular analysis. The patient, a 63 year-old man, underwent a subtotal resection of a left temporal lobe GBM, which was subjected to the set of molecular diagnostic analyses that are standard for such cases at Massachusetts General Hospital, including SNaPshot genotyping and tests for common gene amplifications, translocations and methylation (22, 23). Only focal amplification of EGFR was observed. Within 14 months of the initial diagnosis, a recurrent lesion was resected in the right temporal lobe, and routine screening revealed bilateral pulmonary nodules and hilar lymphadenopathy. Repeated SNaPshot analysis of the tumor revealed only low-level EGFR amplification (<15 copies). The patient expired 22 months after the initial diagnosis. Histopathologic and molecular analysis of a lymph node biopsy and of pulmonary nodules collected at autopsy confirmed metastatic EGFR-amplified GBM (Supplemental Figure 5A).

Analysis of peripheral blood samples obtained 12 months after diagnosis revealed a high number of CTCs (48.2 cells per ml), which were similar to the primary and metastatic tumors in their pleomorphic morphology and presence of EGFR amplification (Supplemental Figure 5B). RNA-ISH analysis of the recurrent intracranial GBM showed an admixture of N (19.0%), N/M (65.3%) and M (15.7%) cells (Figure 4D). In contrast, M-only cells comprised the majority of GBM cells present in the metastatic left hilar lymph node (61.6%) and in pulmonary metastases (53.9%) (Figure 4D).

To test for genetic lesions that may contribute to metastatic dissemination of GBM, we subjected the primary lesion, the major right pulmonary metastasis and normal CNS tissue (as germline control) to next generation sequencing of 1,000 cancer-associated genes. Identified somatic mutations were then tested in multiple independent visceral lesions, generating a schematic representation of clonal progression for metastatic GBM. Enrichment

of a *PDGFRβ* mutation from 3.5% allele frequency in the primary tumor, to approximately 50% allele frequency in all five metastatic lesions was indicative of a mutant *PDGFRβ* tumor initiating subpopulation for extracranial metastases (Figure 4E). Acquired mutations in *EGFR, RB1*, and *SETD2* were absent in the primary tumor but were present in all five metastatic sites (i.e. "truncal mutations") (Figure 4E). Additional mutations in *PHF6, GSK3β, JAK3*, and *VRK3* were restricted to more distal branches, consistent with the evolution of secondary mutations from metastatic lesions in the lower lobe of the right lung to more distal lesions in the upper lobe of the left lung and chest wall (Figure 4E). Taken together, while no singular genetic abnormality may account for metastatic dissemination of GBM cells in this case, the relatively high number of CTCs, the high mesenchymal expression pattern of CTCs, and acquired mutations in oncogenic pathways may have contributed to this phenomenon.

Discussion

We report that patients with glioblastoma have circulating brain tumor cells within the peripheral blood. Since these cells are very rare and express a subset of markers present in primary GBMs, their identification was made possible by our development of a "negative-depletion" CTC-iChip, which effectively removes leukocytes from blood samples, enriching for CTCs without requiring tumor cell-specific capture antibodies (7). Validation of CTCs as being derived from GBMs include mCherry-tagging of patient-derived brain tumor cells orthotopically injected into a mouse brain tumor model, staining of primary CTCs from GBM patients using a panel of glioma markers (STEAM), and demonstration of EGFR gene amplification in CTCs from cases known to have such amplifications in the primary tumor. Molecular characterization of expression markers within individual GBM CTCs identified enrichment for mesenchymal transcripts and reduction of neural differentiation markers, pointing to a subset of cells within primary GBM tumors with such profiles, which were identifiable by RNA-ISH. Together, these observations raise the possibility that a subset of primary GBM cells, expressing abundant mesenchymal transcripts, gain access to blood vessel lumina within the brain and circulate in the systemic vasculature. Further, the identification of CTCs in patients with GBM raises the possibility that their detection and analysis may ultimately be of clinical utility in monitoring patients with this relatively inaccessible tumor.

Of the 33 GBM patients enrolled in our study, however, only 39% had detectable CTCs in at least one of an average 2.6 venous blood draws. Patients with progressive disease tended to have a greater frequency of CTCs. Based on our limited dataset, we could not determine whether surgical or radiation-induced disruption of the blood brain barrier (BBB) enhances CTC dissemination, but we note that one of four patients tested before either surgery or radiation had a small number of CTCs in the peripheral blood, pointing to the ability of GBM cells to intravasate in the absence of therapy-mediated BBB disruption. With further improvements in the sensitivity of detection, CTC analyses could play a role in disease monitoring, for instance in the clinical setting of "pseudoprogression", where radiographic imaging frequently fails to distinguish between treatment-related responses and tumor recurrence, sometimes necessitating a repeat brain biopsy (2).

While not of immediate clinical utility, the analysis of GBM CTCs provides biological insights into the process of GBM invasion and the apparent paradox of rare systemic metastases in a highly invasive and angiogenic cancer. Recent expression profiling of bulk primary tumor RNA has suggested distinct subtypes of primary GBM, defined in part by expression of neural/proneural (N) differentiation versus mesenchymal (M) markers (10, 14). Our RNA-ISH studies provide further resolution at the level of single cells and point to geographically distinct M tumor cell subpopulations within all GBMs analyzed. M-GBM cells are predominant within white matter tracts in the brain, which are sites classically associated with invasion of GBM cells and which thus serve as a conduit for the dissemination of GBM cells to different parts of the brain. In contrast to the evident M-GBM cells, few N-GBM cells are evident within these white matter tracts. In addition, M-GBM cells are enriched among the GBM cells that constitute the characteristic palisades surrounding necrotic foci in the primary tumor. These histological structures are thought to harbor stem-like tumor cells which serve as a reservoir of GBM self-renewal and during disease progression (19-21). The coincidence of mesenchymal transcript expression within this cancer stem cell niche suggests a role for a process similar to Epithelial-to-Mesenchymal Transition (EMT) in GBM homeostasis and systemic circulation. Such a cell fate transition presumably reflects the aberrant activation of a developmental program, by which neuro-epithelial precursors migrate to form neural crest derivatives (24). Characteristic regulators of mesenchymal cell fate, including TWIST1, SNAI2 and elements of TGF-β and NF-κB signaling pathways, are overexpressed in the Mesenchymal subset of GBM (10, 14, 25, 26), which is associated with resistance to standard therapies and a poor prognosis (15). Individual GBMs have been reported to switch among the major subtypes in response to therapy and during progression (14, 16). Our RNA-ISH studies of primary GBMs are consistent with these findings, suggesting that subpopulations coexist within a single tumor and that such apparent cell fate switching may result in part from the effect of selective pressures on heterogeneous cancer cell populations (27).

All of the GBM CTCs detected in patient samples as well as patient-derived xenografts shared a mesenchymal expression profile. Similarly, in the index GBM patient with multiple systemic metastases, all of these extracranial lesions were predominantly mesenchymal. While limited in the number of events observed, these findings are consistent with M-GBM cells being more invasive into the bloodstream and on rare occasion, competent to produce metastases outside of the brain. Brain tumors present the ultimate paradox in the classical “seed versus soil” debate on the relative roles of intrinsic tumor cell biology versus host microenvironment in the distant spread of cancer (4). GBM cells display genetic lesions that are similar to those of epithelial cancers, invade diffusely within the brain and mediate a profound angiogenic reaction within the primary tumor, with areas of necrosis and hemorrhage (2, 10, 14). Indeed, our detailed genetic analysis of the index patient demonstrate EGFR copy gain in the primary tumor and acquisition of both dominant “truncal” mutations and secondary “branch” mutations as metastatic lesions progressed from one to multiple sites. The nature of these mutations, as well as their oligoclonal progression is analogous to those reported for epithelial cancers such as breast and kidney (28, 29). These acquired mutations present in metastatic lesions are likely to confer additional

invasive properties, consistent with those proposed in epithelial cancers that metastasize more frequently.

Despite the detection of GBM CTCs, the absence of systemic metastases in the majority of patients with GBM is unexplained. While the number of CTCs detectable in the blood of patients with GBM is low, it is within the broad range observed using microfluidic platforms with other types of cancer all of which give rise to systemic metastases (7, 12). As such, it suggests that GBM cells are able to enter the systemic vascular system and survive there long enough for detection, but that they are only rarely capable of initiating gross metastatic lesions in visceral organs. It is possible that GBM cells require critical neural-specific growth factors that are absent outside the brain. We were unable to identify autocrine activation of such pathways within the visceral metastatic lesions of the index patient, using growth factor receptor arrays (data not shown). Alternatively, immune-mediated suppression of GBM cells harboring epitopes that are usually masked by the blood brain barrier and hence considered foreign may underlie the general failure of GBM proliferation in visceral organs. Both of these models warrant further investigation. Together, the identification of GBM CTCs and their detailed characterization may provide insight into the invasive properties of these aggressive brain tumors, ultimately identifying new therapeutic opportunities to suppress proliferation of primary GBMs.

Methods

See Supplemental Material for a full description of Methods

Primary GBM Culture

Early passage, GBM8 and GBM24 cells were derived from patient specimens, modified by lentiviral infection to stably express luciferase and mCherry, and were maintained *in vivo* and in neurosphere culture conditions as previously described (8, 30). Cultures were verified periodically by DNA-FISH for known copy aberrations and routinely tested and all were negative for mycoplasma infection (8).

CTC Isolation from Clinical Specimens

Consenting patients with WHO grade IV glioblastoma receiving treatment at the Massachusetts General Hospital (Boston, MA) were accrued for this study according to an institutional review board (IRB)-approved protocol. Whole blood (10-20 ml) was collected on one or more occasions from a total of 34 patients and from 5 healthy volunteers, under a separate IRB-approved protocol, for CTC analysis as previously described (7). Cells enriched the CTC-iChip were collected in buffered solution and immediately spun onto glass slides (Shandon EZ Megafunnel, Thermo Scientific) for STEAM immunofluorescence (7), or processed for fluorescence guided single cell micromanipulation (see supplemental methods for a full description).

RNA Expression Analyses of Single Cells and FFPE Tissue Specimens

RNA extracted from FFPE tissues (AllPrep DNA/RNA FFPE kit, Qiagen) and from lysed single cells were reverse transcribed and processed for Fluidigm Single Cell Gene

Expression analysis as described (7, 31). A brief pre-amplification of target transcripts was performed using a custom panel of 49 validated gene primer pairs (DELTAgene Assay, Fluidigm Corp.), followed by qPCR analysis on a BioMark HD Real-Time PCR System (Fluidigm Corp.). Dual color RNA-ISH of FFPE tissues was performed using custom designed QuantiGene ViewRNA probes (Affymetrix) against neural (*ASCL1*, *GFAP*, *OLIG2*, *PDGFRA*, and *SOX2*) and mesenchymal GBM subtype transcripts (*SERPINE1*, *TGFB1*, *TGFBR2*, and *VIM*) (see supplemental methods for a full description of these assays).

Supplementary Material

Refer to Web version on PubMed Central for supplementary material.

Acknowledgments

The authors thank Drs. S. Stott, G. Mohapatra, J. Deitrich, J. Walsh, P. Sphuler and A. Shah for reagents and technical support; C. Koris and J. Brown for coordinating patient sample procurement; and to the patients and their families for their participation in this study.

Grant Support: This work was funded by grants from the US National Institutes of Health K12CA090354, P50CA165962, and NIHLRP (to T.T. Batchelor, D.A. Haber and B.N. Nahed); B*Cured (to B.N. Nahed); Voices Against Brain Cancer (to B.N. Nahed); a Stand Up To Cancer Dream Team Translational Cancer Research Grant (SU2C-AACR-DT0309, to D.A. Haber, M. Toner, and S. Maheswaran) (Stand Up To Cancer is a program of the Entertainment Industry Foundation administered by the American Association for Cancer Research); and Howard Hughes Medical Institute (to D.A. Haber).

References

1. Louis DN, Ohgaki H, Wiestler OD, Cavenee WK, Burger PC, Jouvet A, et al. The 2007 WHO classification of tumours of the central nervous system. Acta neuropathologica. 2007; 114:97–109. [PubMed: 17618441]
2. Omuro A, DeAngelis LM. Glioblastoma and other malignant gliomas: a clinical review. JAMA : the journal of the American Medical Association. 2013; 310:1842–50.
3. Smith DR, Hardman JM, Earle KM. Contiguous glioblastoma multiforme and fibrosarcoma with extracranial metastasis. Cancer. 1969; 24:270–6. [PubMed: 4307749]
4. Fidler IJ. The pathogenesis of cancer metastasis: the ‘seed and soil’ hypothesis revisited. Nature reviews Cancer. 2003; 3:453–8.
5. Yu M, Stott S, Toner M, Maheswaran S, Haber DA. Circulating tumor cells: approaches to isolation and characterization. The Journal of cell biology. 2011; 192:373–82. [PubMed: 21300848]
6. Alix-Panabieres C, Schwarzenbach H, Pantel K. Circulating tumor cells and circulating tumor DNA. Annual review of medicine. 2012; 63:199–215.
7. Ozkumur E, Shah AM, Ciciliano JC, Emmink BL, Miyamoto DT, Brachtel E, et al. Inertial focusing for tumor antigen-dependent and -independent sorting of rare circulating tumor cells. Science translational medicine. 2013; 5:179ra47.
8. Wakimoto H, Mohapatra G, Kanai R, Curry WT Jr, Yip S, Nitta M, et al. Maintenance of primary tumor phenotype and genotype in glioblastoma stem cells. Neuro-oncology. 2012; 14:132–44. [PubMed: 22067563]
9. Tchoghandjian A, Baeza N, Colin C, Cayre M, Metellus P, Beclin C, et al. A2B5 cells from human glioblastoma have cancer stem cell properties. Brain pathology. 2010; 20:211–21. [PubMed: 19243384]
10. Verhaak RG, Hoadley KA, Purdom E, Wang V, Qi Y, Wilkerson MD, et al. Integrated genomic analysis identifies clinically relevant subtypes of glioblastoma characterized by abnormalities in PDGFRA, IDH1, EGFR, and NF1. Cancer cell. 2010; 17:98–110. [PubMed: 20129251]

11. Grzmil M, Morin P Jr, Lino MM, Merlo A, Frank S, Wang Y, et al. MAP kinase-interacting kinase 1 regulates SMAD2-dependent TGF-beta signaling pathway in human glioblastoma. Cancer research. 2011; 71:2392–402. [PubMed: 21406405]
12. Stott SL, Hsu CH, Tsukrov DI, Yu M, Miyamoto DT, Waltman BA, et al. Isolation of circulating tumor cells using a microvortex-generating herringbone-chip. Proceedings of the National Academy of Sciences of the United States of America. 2010; 107:18392–7. [PubMed: 20930119]
13. Stott SL, Lee RJ, Nagrath S, Yu M, Miyamoto DT, Ulkus L, et al. Isolation and characterization of circulating tumor cells from patients with localized and metastatic prostate cancer. Science translational medicine. 2010; 2:25ra3.
14. Phillips HS, Kharbanda S, Chen R, Forrest WF, Soriano RH, Wu TD, et al. Molecular subclasses of high-grade glioma predict prognosis, delineate a pattern of disease progression, and resemble stages in neurogenesis. Cancer cell. 2006; 9:157–73. [PubMed: 16530701]
15. Colman H, Zhang L, Sulman EP, McDonald JM, Shooshtari NL, Rivera A, et al. A multigene predictor of outcome in glioblastoma. Neuro-oncology. 2010; 12:49–57. [PubMed: 20150367]
16. Bhat KP, Balasubramaniyan V, Vaillant B, Ezhilarasan R, Hummelink K, Hollingsworth F, et al. Mesenchymal differentiation mediated by NF-kappaB promotes radiation resistance in glioblastoma. Cancer cell. 2013; 24:331–46. [PubMed: 23993863]
17. Yu M, Bardia A, Wittner BS, Stott SL, Smas ME, Ting DT, et al. Circulating breast tumor cells exhibit dynamic changes in epithelial and mesenchymal composition. Science. 2013; 339:580–4. [PubMed: 23372014]
18. Dong S, Nutt CL, Betensky RA, Stemmer-Rachamimov AO, Denko NC, Ligon KL, et al. Histology-based expression profiling yields novel prognostic markers in human glioblastoma. Journal of neuropathology and experimental neurology. 2005; 64:948–55. [PubMed: 16254489]
19. Brat DJ, Castellano-Sanchez AA, Hunter SB, Pecot M, Cohen C, Hammond EH, et al. Pseudopalisades in glioblastoma are hypoxic, express extracellular matrix proteases, and are formed by an actively migrating cell population. Cancer research. 2004; 64:920–7. [PubMed: 14871821]
20. Brat DJ, Van Meir EG. Vaso-occlusive and prothrombotic mechanisms associated with tumor hypoxia, necrosis, and accelerated growth in glioblastoma. Laboratory investigation; a journal of technical methods and pathology. 2004; 84:397–405.
21. Seidel S, Garvalov BK, Wirta V, von Stechow L, Schanzer A, Meletis K, et al. A hypoxic niche regulates glioblastoma stem cells through hypoxia inducible factor 2 alpha. Brain : a journal of neurology. 2010; 133:983–95. [PubMed: 20375133]
22. Dias-Santagata D, Akhavanfard S, David SS, Vernovsky K, Kuhlmann G, Boisvert SL, et al. Rapid targeted mutational analysis of human tumours: a clinical platform to guide personalized cancer medicine. EMBO molecular medicine. 2010; 2:146–58. [PubMed: 20432502]
23. Chi AS, Batchelor TT, Dias-Santagata D, Borger D, Stiles CD, Wang DL, et al. Prospective, high-throughput molecular profiling of human gliomas. Journal of neuro-oncology. 2012; 110:89–98. [PubMed: 22821383]
24. Sauka-Spengler T, Bronner-Fraser M. A gene regulatory network orchestrates neural crest formation. Nature reviews Molecular cell biology. 2008; 9:557–68.
25. Zarkoob H, Taube JH, Singh SK, Mani SA, Kohandel M. Investigating the link between molecular subtypes of glioblastoma, epithelial-mesenchymal transition, and CD133 cell surface protein. PloS one. 2013; 8:e64169. [PubMed: 23734191]
26. Tso CL, Freije WA, Day A, Chen Z, Merriman B, Perlina A, et al. Distinct transcription profiles of primary and secondary glioblastoma subgroups. Cancer research. 2006; 66:159–67. [PubMed: 16397228]
27. Patel AP, Tirosh I, Trombetta JJ, Shalek AK, Gillespie SM, Wakimoto H, et al. Single-cell RNA-seq highlights intratumoral heterogeneity in primary glioblastoma. Science. 2014; 344:1396–401. [PubMed: 24925914]
28. Navin N, Kendall J, Troge J, Andrews P, Rodgers L, McIndoo J, et al. Tumour evolution inferred by single-cell sequencing. Nature. 2011; 472:90–4. [PubMed: 21399628]

29. Gerlinger M, Rowan AJ, Horswell S, Larkin J, Endesfelder D, Gronroos E, et al. Intratumor heterogeneity and branched evolution revealed by multiregion sequencing. The New England journal of medicine. 2012; 366:883–92. [PubMed: 22397650]

30. Wakimoto H, Kesari S, Farrell CJ, Curry WT Jr, Zaupa C, Aghi M, et al. Human glioblastoma-derived cancer stem cells: establishment of invasive glioma models and treatment with oncolytic herpes simplex virus vectors. Cancer research. 2009; 69:3472–81. [PubMed: 19351838]

31. Powell AA, Talasaz AH, Zhang H, Coram MA, Reddy A, Deng G, et al. Single cell profiling of circulating tumor cells: transcriptional heterogeneity and diversity from breast cancer cell lines. PloS one. 2012; 7:e33788. [PubMed: 22586443]

Significance

GBMs are locally invasive within the brain but rarely metastasize to distant organs, exemplifying the debate over “seed” vs “soil”. We demonstrate that GBMs shed CTCs with invasive mesenchymal characteristics into the circulation. Rare metastatic GBM lesions are primarily mesenchymal and show additional mutations absent in the primary tumor.

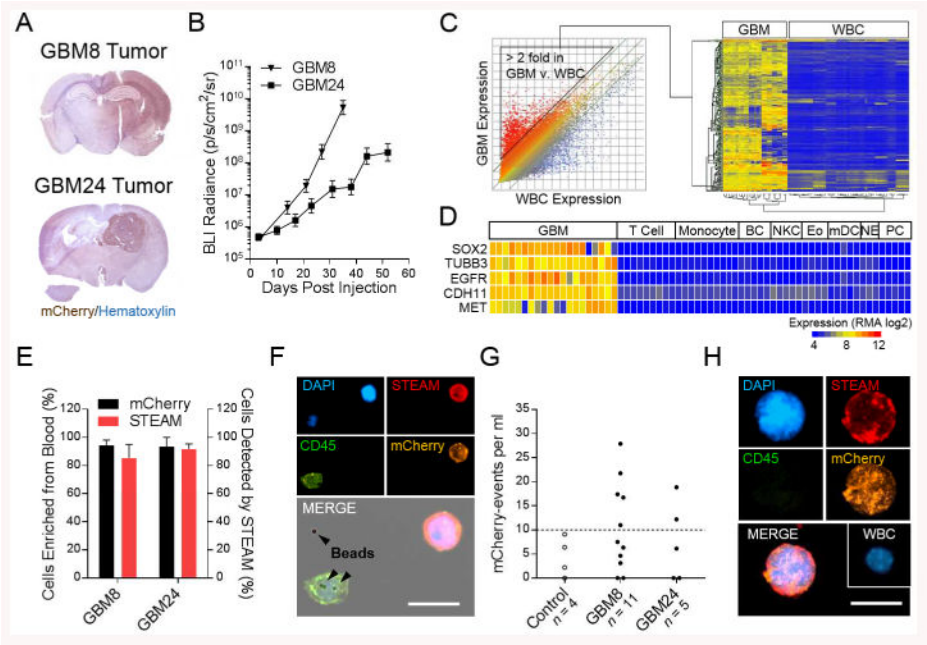

Figure 1.

Enrichment and detection of CTCs from orthotopic xenograft models of GBM. **A**, immunohistologic analysis of coronal sections showing mCherry expressing GBM8 and GBM24 tumor xenografts. **B**, bioluminescence imaging of GBM xenografts (n = 6). **C**, genome-wide expression of GBM and WBCs identifies tumor specific markers. Left panel: genes plotted by average expression in GBM and WBCs from publically available microarrays (GSE15824: 15 GBM tumors and 5 GBM cell lines; GSE33331: 10 $CD14^+$ monocyte, 5 mature dendrocyte (mDC), 4 eosinophil (Eo), 5 $CD19^+$ B cell (BC), 5 $CD4^+$ and 5 $CD8^+$ T cell (T Cell), 5 $CD56^+$ natural killer T cell (NKC), 3 neutrophil (NE) and 5 plasma dendrocyte (PC) samples). Right panel: an unsupervised hierarchical cluster analysis of the genes expressed two-fold greater in tumor cells versus WBCs. **D**, expression heatmap of candidate CTC markers in GBM and WBCs. **E**, bar graph showing the recovery of $mCherry^+$ GBM cells from GBM8 and GBM24 tumor cell spiked blood samples processed through the CTC-iChip (left y-axis) and stained with the STEAM antibody cocktail (right y-axis) (n = 4). **F**, images of a GBM8 cell and WBC isolated from GBM8 cell line spiked blood processed through the CTC-iChip and stained with DAPI, mCherry and the STEAM cocktail (single color images: x20 magnification, merged image: x40 magnification). Free and WBC bound CD45 antibody-conjugated immunomagnetic beads are shown (black arrows) in the merged immunofluorescence and brightfield images in the bottom panel. **G**, quantification of $mCherry^+$ cells isolated from sham-operated and GBM8 and GBM24 xenografted mice. The dotted line marks the baseline set for CTC detection based on mCherry, STEAM and CD45 staining of blood analyzed from control mice. **H**, representative images of a $STEAM^+/mCherry^+$ CTC and a $CD45^{-/low}$ WBC isolated from the blood of a mouse bearing a GBM8 xenograft.

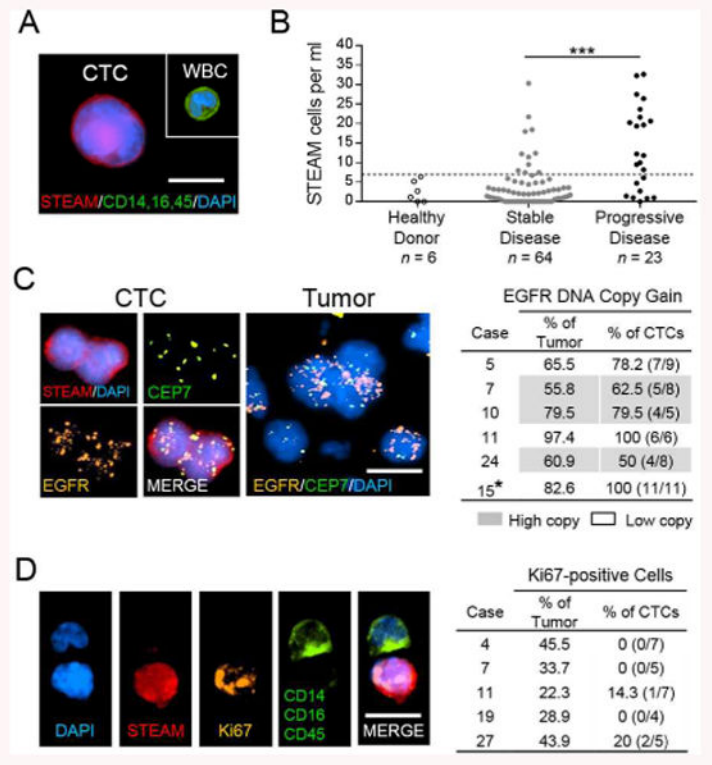

Figure 2.

Identification of CTCs in the peripheral blood of GBM patients. **A**, a representative immunofluorescence image of a STEAM$^+$ CTC alongside a WBC isolated from GBM patient blood. Scale bar = 20 μm. **B**, quantification of STEAM$^+$ cells in healthy donor samples established a CTC detection threshold of 7 STEAM$^+$ cells per ml. Quantification of STEAM$^+$ cells in 64 blood samples drawn from 21 patients with stable disease and 23 blood samples from 12 patients with progressive disease (***$P < 0.001$). **C**, left panels: representative images of a CTC stained with the STEAM antibody cocktail (red) and analyzed by DNA-FISH using probes against centromere 7 (CEP7, green) and EGFR (orange). Center panel: CEP7/EGFR DNA-FISH in matched primary tumor cells from the patient is shown. Right panel: table of the frequency of EGFR-amplified cells in primary tumors ($n = 5$) and matched STEAM$^+$ CTCs ($n = 36$). Cells with focal EGFR copy gain (≥ 10 copies) are shaded in grey. Asterisk signifies results from a patient with metastatic GBM, presented in full later in the paper. Scale bar = 20 μm. **D**, left panels: a STEAM$^+$ CTC (red) expressing nuclear Ki67 (orange). A CD45 stained WBC is shown (green). Right panel: table of the frequency of Ki67$^+$/STEAM$^+$ CTCs ($n = 28$) and Ki67 positive tumor cells in the matched tumor specimens ($n = 5$). Scale bar = 20 μm.

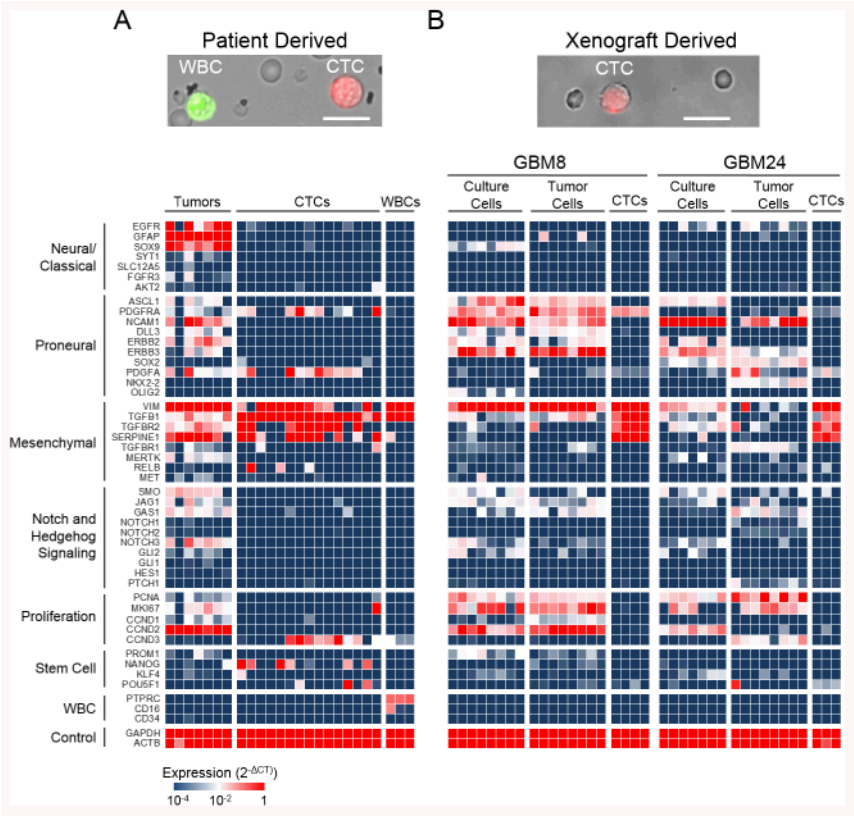

Figure 3.

Expression analysis of single GBM CTCs and primary tumor cells. **A**, upper panel: phase contrast/immunofluorescence image a GBM CTC (red), red blood cells and a WBC (green) stained in solution after iChip-enrichment of patient blood (Scale bar = 20 μm). The GBM CTC was picked by microscopy guided single cell isolation. Lower panel: a heatmap of gene expression patterns (normalized to GAPDH) in individual GBM CTCs (*n* = 15), primary tumor samples (*n* = 7) and WBCs (*n* = 3) derived from 7 GBM patients. **B**, upper panel: an iChip-enriched mCherry^{+} CTC obtained from mice carrying the GBM8 xenograft (red) prior to isolation for molecular analysis. Lower panel: expression heatmap of single cells isolated from GBM8 and GBM24 neurosphere cultures (*n* = 8 and 7, respectively), xenografts (*n* = 8, each) and CTCs (*n* = 4 and 3, respectively). Scale bar = 20 μm. The genes analyzed by Fluidigm qPCR are shown on the left.

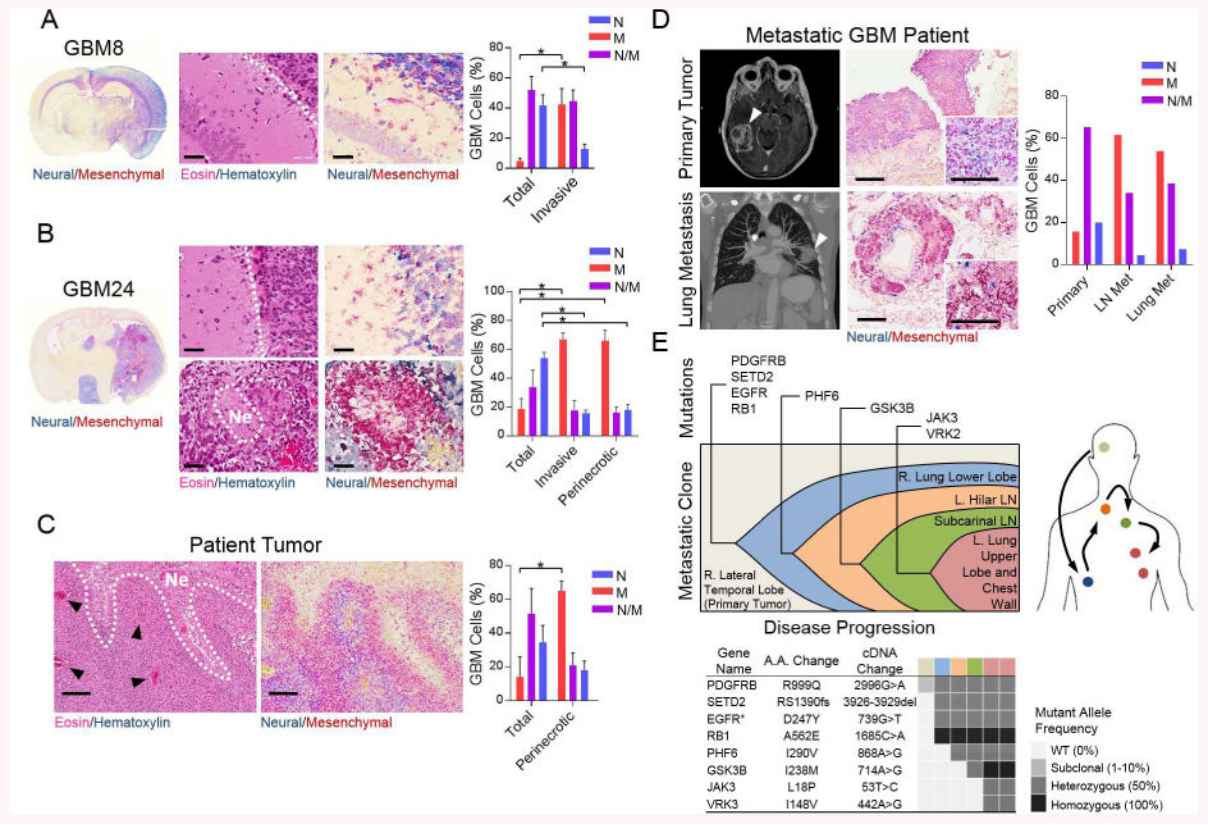

Figure 4.

RNA-ISH analysis of GBM xenografts, patient and metastatic primary GBM samples. **A**, left panel: RNA-ISH of Mesenchymal (M, red) and Neural (N, blue) genes in a coronal section shows the diffuse pattern of the GBM8 xenograft. Center and right panels: H&E and RNA-ISH images of GBM8 tumor cells invading the hippocampal strata. The bar graph on the right shows the percentage of M, N and N/M populations in the total GBM8 xenograft and those invading the hippocampus quantified after RNA-ISH analysis (right panel, $n = 3$, $^*P < 0.05$). Scale bars = 50 μm. **B**, left panel: RNA-ISH of a coronal section showing the GBM24 xenograft. Center and right panels: H&E and RNA-ISH images of GBM24 tumor cells invading the hippocampus and residing near necrotic (Ne) foci. Bar graph on the right shows the M, N, and M/N composition of total, hippocampal invading and perinecrotic GBM24 tumor cells (right panel, $n = 3$, $^*P < 0.05$). Scale bars = 50 μm. **C**, left panel: H&E of primary tumor sample depicting characteristic tumor necrosis (Ne), adjacent palisading cells (dotted line) and hyper-microvascularization (black arrows). Center panel: RNA-ISH of the same tissue section depicts greater mesenchymal over neural gene expression in perinecrotic tumor cells. Bar graph on the right shows the M, N, and M/N composition of total tumor cells and perinectrotic tumor cells following RNA-ISH analysis of 6 patient biopsies ($^*P < 0.05$). Scale bar = 200 μm. **D**, left panels: cranial and thoracic MRIs of primary and metastatic tumor (white arrows) from an index patient (Patient 15). Center panels: RNA-ISH images (x10 magnification, x20 magnification inserts) of the primary tumor and metastatic GBM cells surrounding a bronchiole. Bar graph on the right shows quantification of M, N, and M/N tumor cells in the primary tumor, hilar lymph node

metastasis (LN met) and lung metastasis. Scale bars = 200 μm. **E**, upper panel: a diagram of the clonal metastatic spread of GBM derived from the mutational analysis of primary and metastatic sites. Lower panel: depiction of the frequency of specific mutant alleles in each lesion (color coded to diagram in upper panel).